Flame ignition in a premixed turbulent flow

By T. J. Poinsot[1]

A preliminary study of the ignition of a premixed flame front in a two-dimensional turbulent flow is presented. Flame ignition is studied using full numerical simulation including heat release, variable fluid properties, and one-step Arrhenius chemistry. The effects of turbulence on the flame growth as well as the effects of the flame on the surrounding turbulence are described. It is shown that, if combustion is successfully initiated, the initial growth is always laminar-like mainly because of dilatation effects through the flame front. Later, the turbulent fluctuations begin to wrinkle the flame and transition to turbulent propagation takes place. The influence of numerical parameters such as boundary and initial conditions is considered. The effect of Lewis number is evidenced by comparing the growth of two flames with the same flame speeds in the same turbulence but with different Lewis numbers ($Le = 1.2$ and $Le = 0.53$)

1. Background and objectives

Flame ignition in most industrial devices takes place in a turbulent situation (Hamai et al. (1986), Pischinger and Heywood (1990), Baritaud (1987)). Energy is deposited in the turbulent gas using a spark (in piston engines, for example), chemical reaction begins when the temperature reaches a sufficient level and a flame kernel is initiated. The subsequent growth (or death) of this kernel is the central question of ignition studies. Studies of minimum energy and times for ignition have been performed in *laminar flows* using asymptotic methods (Champion et al. (1986), Champion et al. (1988)), numerical methods (Frendi and Sibulkin (1990), Ko and Arpaci (1991), Maly and Vogel (1978), Maly (1981), Tromans and Furzeland (1986), Sloane (1990)) and experiments (Ko et al. (1991), Champion et al. (1986), Sloane (1990)). Although much is known about ignition processes in laminar flows, the application of these studies to practical cases is limited by the unknown effects of turbulence on these processes. Only a few results on ignition in *turbulent flows* are available. Research scientists working in the field of reciprocating engines have been quite active in this field (Baritaud (1987), Pischinger and Heywood (1990), Boston et al. (1984)) but the complexity of flow fields and the difficulty of performing measurements inside piston engines makes some of the relevant information difficult to extract from these studies (the turbulence characteristics, for example, are complex and difficult to estimate). As indicated by Pischinger and Heywood (1990), few multi-dimensional models simulating spark-generated flame ignition are available today. Models based on stochastic approaches (Pope and Cheng (1986)) or on flame wrinkling predictions (Thomas (1986), Mantel and Borghi (1991)) have

1 Permanent address: C.N.R.S., Ecole Centrale de Paris

been proposed but fundamental information to test these models is lacking in most cases. The goal of this study is to consider feasability and efficiency of a full Direct Numerical Simulation to provide precise data on flame growth in a turbulent flow.

In the present study, the modeled system includes heat release, variable fluid properties, and simple chemistry in two–dimensional turbulence. While it is recognized that two–dimensional turbulence differs from three–dimensional turbulence (e.g., Herring et al. (1974), Lesieur (1987)), the response of the flame front during its growth in a two-dimensional computation should be generic, even if detailed statistical correlations (especially of small–scale quantities) differ quantitatively from what would be found in three dimensions. Restricting the simulations to two dimensions permits a much wider dynamic range of scales to be computed, so that, for example, higher turbulence Reynolds numbers can be simulated while still resolving the flame structure (Haworth and Poinsot (1990)). The present results are also used as a tool to develop techniques which will be utilized in three–dimensional computations. The effects of energy deposition, the influence of boundary conditions on turbulence, the effects of Lewis number may be assessed first in a two-dimensional case before implementation in a three-dimensional situation.

We will present first the equations which are solved and the configuration (Section 2). A typical example of ignition will be given in Section 3. Numerical effects will be considered in Section 4. Because we study compressible flows with strong dilatation, the boundary conditions must allow acoustic waves as well as flow to leave the computation domain. Adequate boundary conditions to treat this problem will be discussed and tested in Section 4.1. The influence of initial turbulence conditions will be discussed in Section 4.2. The effects of thermodiffusive instabilities (controlled by the Lewis number Le) during ignition are tested in Section 5.

2. Equations and configuration

The basic equations and the numerical algorithm used in this study are described in Poinsot et al. (1991). We consider a compressible viscous reacting flow. The chemical reaction is represented by a single–step mechanism,

$$R \quad \text{(reactants)} \quad \rightarrow P \quad \text{(products)}, \tag{1}$$

and the reaction rate $\dot{w}_R$ is expressed as,

$$\dot{w}_R = B\rho Y_R \ \exp\left(-\frac{T_a}{T}\right). \tag{2}$$

This can be interpreted as a binary reaction where one of the reactants (Y_R) is always deficient. It is convenient to follow Williams (1988) and cast this expression in the form,

$$\dot{w}_R = B\rho Y_R \exp\left(\frac{-\beta(1-\Theta)}{1-\alpha(1-\Theta)}\right). \tag{3}$$

Here Θ is the reduced temperature, $\Theta = (T - T_1)/(T_2 - T_1)$, where T_1 is the fresh gas temperature and T_2 is the adiabatic flame temperature for unity Lewis number.

The activation energy is T_a, and the coefficients B, α, and β are, respectively, the reduced pre–exponential factor, the temperature factor and the reduced activation energy,

$$\mathcal{B} = B\exp(-\beta/\alpha), \quad \alpha = (T_2 - T_1)/T_2, \quad \text{and} \quad \beta = \alpha T_a/T_2. \tag{4}$$

The mass fraction of the reactants Y_R may be conveniently nondimensionalized by the initial mass fraction of reactants Y_R^o in the fresh gases, $\widetilde{Y} = Y_R/Y_R^o$, so that $\widetilde{Y}$ varies from 1 in the fresh gases to 0 in the burnt gases. Fluid properties follow the equations of state,

$$\rho = \rho_1(pT_1/p_1T)\ ,\ \mu = \mu_1(T/T_1)^b\ ,$$

$$Le = \lambda/\rho D c_p = \text{constant}\ ,\ Pr = \mu c_p/\lambda = \text{constant}\ , \tag{5}$$

where μ, λ, and D are molecular diffusivities of momentum, internal energy, and species, respectively. Here a subscript 1 refers to reference properties in the fresh gases.

Using these assumptions and a Cartesian frame of reference, the conservation equations for compressible flows are solved using a high–order finite difference scheme. The numerical accuracy is sixth–order in space and third–order in time (Lele (1989)). Boundary conditions are specified using the NSCBC method (Poinsot and Lele (1991)).

The calculations are initialized with reactants everywhere in the square domain. For the turbulent cases, the initial velocity field (turbulence spectrum) is specified at $t = 0$: the system is then allowed to evolve in time. After a certain delay t_{delay} (to let turbulence evolve to a meaningful spectrum), combustion is initiated in the middle of the computation box. This is done by adding a source term in the energy equation. The form of this term is the following:

$$Q_i = Q exp(-\frac{r^2}{2R^2}), \tag{6}$$

where r is the distance of a given point to the center of the box and R is the size of the simulated spark. Q is a constant. This source term is maintained during a time $t_{ignition}$ and then switched off.

For a fixed chemistry model, the control parameters in this simulation are:
– ratio of initial RMS turbulence intensity u' to the undisturbed laminar flame speed s_l^0;
– ratio of initial turbulence integral length scale to laminar flame thickness δ_{l2}. Two integral length scales may be used : the two-point correlation length l_1 or a length defined from the turbulence characteristics: $l_2 = 0.4k^{(3/2)}/\epsilon$ (the kinetic energy in these 2D cases is $k = u'^2$);
– ratio of spark duration $t_{ignition}$ to typical flame time t_{flame} ;
– ratio of spark size R to typical flame thickness δ_{l2} and
– ratio of spark power Q deposition to typical flame power Q_{flame}.

We do not scale the spark characteristics with critical values obtained from asymptotic studies (Champion et al. (1986), Champion et al. (1988)) because these values might not be relevant for turbulent cases. The flame thickness is estimated by

$$\delta_{l2} = \nu / s_l^0, \tag{7}$$

The flame time is

$$t_{flame} = \delta_{l2}/s_l^0 = \nu/{s_l^0}^2. \tag{8}$$

Note that δ_{l2} is close to the reaction zone thickness and therefore smaller than the real thermal thickness δ_{l1} defined by $\delta_{l1} = (T_2 - T_1)/(dT/dx)_{max}$. It is used here because of simplicity and because many authors use it instead of δ_{l1}.

The flame power per unit volume is defined by $Q_{flame} = \rho_{fresh} C_p (T_2 - T_1)/t_{flame}$.

The initial spectrum is given by two parameters: the RMS velocity u' and the length scale of the most energetic vortices L_i:

$$E(\kappa) = C(\kappa/\kappa_i)^4 exp(-2(\kappa/\kappa_i)^2) \tag{9}$$

where κ is the wave number and κ_i corresponds to the most intense wave number, i.e. $\kappa_i = 2\pi/L_i$. The constant C is chosen to satisfy the constraint $k = u'^2 = \int_0^\infty E(\kappa) d\kappa$ and is $C = 32/3\sqrt{2/\pi}\ \ u'^2/\kappa_i$.

The values of these parameters for some of the runs performed are given in Table I.

Table I. Turbulence and flame parameters for ignition problems.
(L is the unit length in the code given by the Reynolds number $Re = Lc/\nu$)
(c is the sound speed and ν the kinematic viscosity)

←	Turbulence		data		→	←	Flame	data	→
Run	X_{max}/L	u'/c	L_i/L	l_1/L	l_2/L	s_L^0	δ_{l1}/L	δ_{l2}/L	Lewis
V1	9	0.1	0.7	0.24	0.4	0.0108	0.237	0.046	1.2
V2	9	0.1	0.7	0.24	0.4	0.0108	0.237	0.046	1.2
V3	9	0.1	0.7	0.24	0.4	0.0108	0.237	0.046	1.2
V4	9	0.05	0.7	0.24	0.2	0.0108	0.237	0.046	1.2
V5	9	0.05	1.4	0.48	0.80	0.0108	0.237	0.046	1.2
V6	9	0.1	1.4	0.48	1.61	0.0108	0.237	0.046	1.2
V7	9	0.05	2.1	0.76	0.9	0.0108	0.237	0.046	1.2
V8	9	0.1	0.7	0.24	0.4	0.0108	0.237	0.046	1.2
V9	9	0.1	0.7	0.24	0.4	0.0108	0.237	0.046	1.2
V10	9	0.1	0.7	0.24	0.4	0.0108	0.237	0.046	1.2
VL1	14	0.1	2.1	0.71	3.6	0.0108	0.237	0.046	1.2
VL2	14	0.1	2.8	0.98	6.1	0.0108	0.237	0.046	1.2
W4	9	0.1	0.7	0.24	0.4	0.0090	0.285	0.055	0.53

Table II contains the reduced parameters and the ignition characteristics. The length ratios L_i/δ_{l2} and l_1/δ_{l1} correspond to maximum and minimum values of a ratio of integral turbulent scale to chemical scale. The large difference between these two values shows how careful one must be when dealing with comparisons between experiment and computation, for example. It must also be noted that all integral lengths grow rapidly when the computation proceeds so that ratios between turbulent and chemical lengths given in Table II are minimum values which increase during computation by a factor of 3 to 4. In the same way, two Reynolds numbers have been reported in Table II: one is based on the two-point integral scale l_1 and the other one on the most energetic scale L_i in the initial spectrum. Because the initial turbulence is not in equilibrium, large differences may be found between both estimates and one has to be careful about which number is actually used to compare with experimental data.

The Damkohler number reported in Table II is defined as $Da = \tau_{turb}/\tau_{chem} = \frac{l_2/u'}{\delta_{l2}/s_L^0}$. Other runs made with different initial spectra have been made and are available at CTR but not reported here. Typical grids contain 257 by 257 or 385 by 385 points.

Table II. Reduced parameters and ignition characteristics for ignition problems.

Run	u'/s_L^0	L_i/δ_{l2}	l_2/δ_{l2}	l_1/δ_{l1}	l_2/δ_{l1}	Da	$u'L_i/\nu$	$u'l_1/\nu$	$\frac{t_{ign}}{t_{flame}}$	$\frac{Q}{Q_{flame}}$
V1	9.26	15.2	8.69	1.01	1.68	0.94	140	48	0.5	3.5
V2	9.26	15.2	8.69	1.01	1.68	0.94	140	48	0.5	4.5
V3	9.26	15.2	8.69	1.01	1.68	0.94	140	48	0.5	5.5
V4	4.63	15.2	4.34	1.01	1.68	0.93	70	24	0.5	5.5
V5	4.63	30.4	17.4	2.02	3.38	3.84	140	48	0.5	5.5
V6	9.26	30.4	35.	2.02	6.79	3.77	280	96	0.5	5.5
V7	4.63	45.6	19.6	3.21	3.80	4.23	210	76	0.5	5.5
V8	9.26	15.2	8.69	1.01	1.68	0.94	140	48	0.5	5.5
V9	9.26	15.2	8.69	1.01	1.68	0.94	140	48	0.5	5.5
V10	9.26	15.2	8.69	1.01	1.68	0.94	140	48	0.5	5.5
VL1	9.26	45.6	78.3	3.12	15.2	8.46	210	142	0.5	5.5
VL2	9.26	60.9	129.8	4.13	25.7	14.	420	196	0.5	5.5
W4	11.1	12.7	7.27	0.84	1.40	0.66	140	48	0.5	5.5

Parameters which were the same for all runs are summarized in Table III (L is the unit length in the code given by the Reynolds number based on sound speed : $Re = Lc/\nu$). For all the present runs, the ignition delay t_{delay} was zero (see Section 4.1).

Table III. Fixed parameters for all simulations.

cL/ν	α	β	Λ	b	Pr	R/L	t_{delay}
2000	0.75	8.00	146.	0.76	0.75	0.08	0.

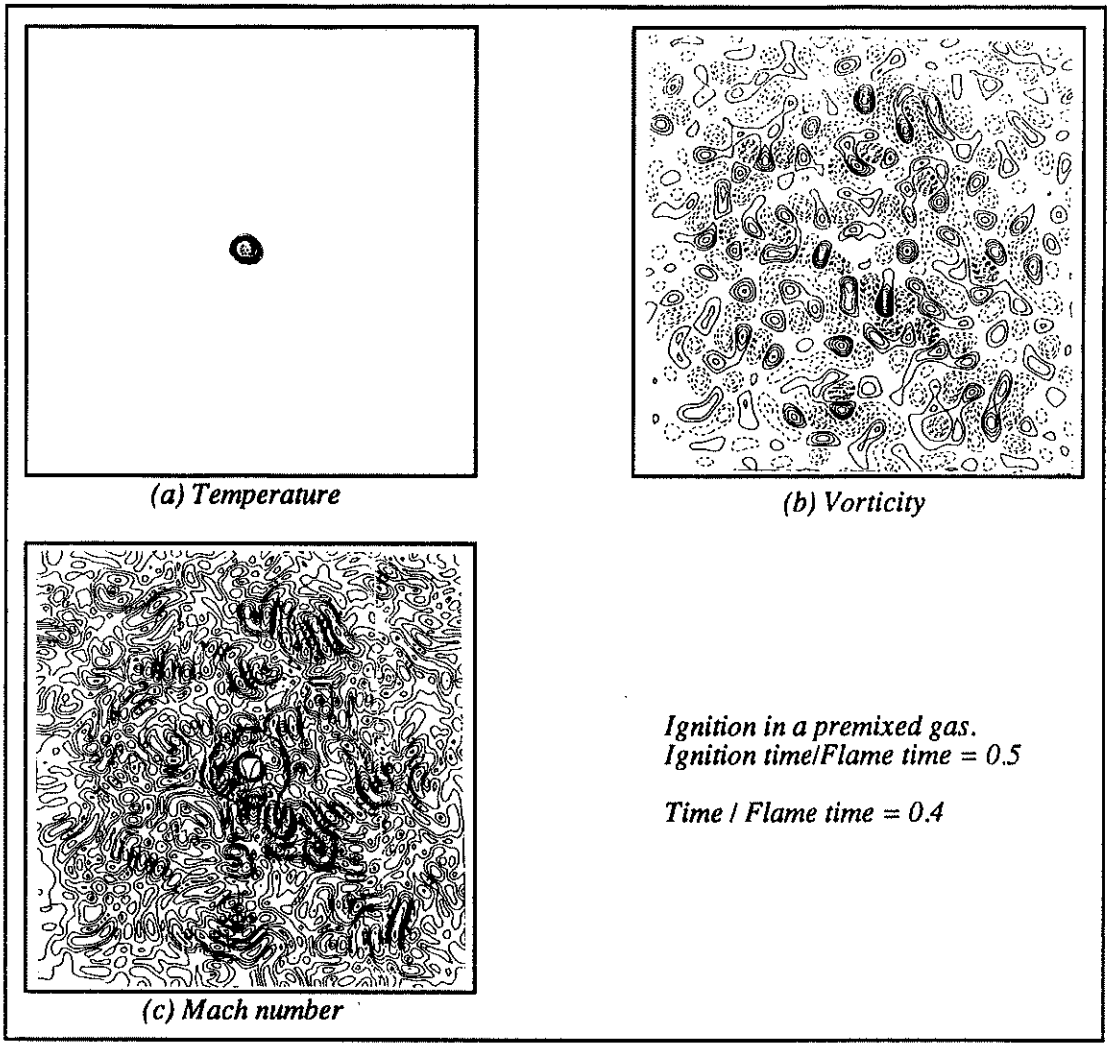

FIGURE 1. Ignition example for $Le = 1.2$: $t/t_{flame} = 0.4$

3. Example of DNS of flame initiation

Typical contours of temperature, Mach number and vorticity are shown in Figures 1, 2, 3 and 4 for a test case (Run V4 in Tables I and II). Figures 1 to 4 correspond respectively to $t/t_{flame} = 0.4$, 0.8, 4 and 6. In terms of initial turn-over

times, this means $t/t_{integral} = u't/l_2 = 0.34$, 0.68, 3.44 and 5.28. The ignition delay t_{delay} is 0 and the ignition time $t_{ignition}$ is $0.5t_{flame}$. The ignition power is $Q = 5.5Q_{flame}$.

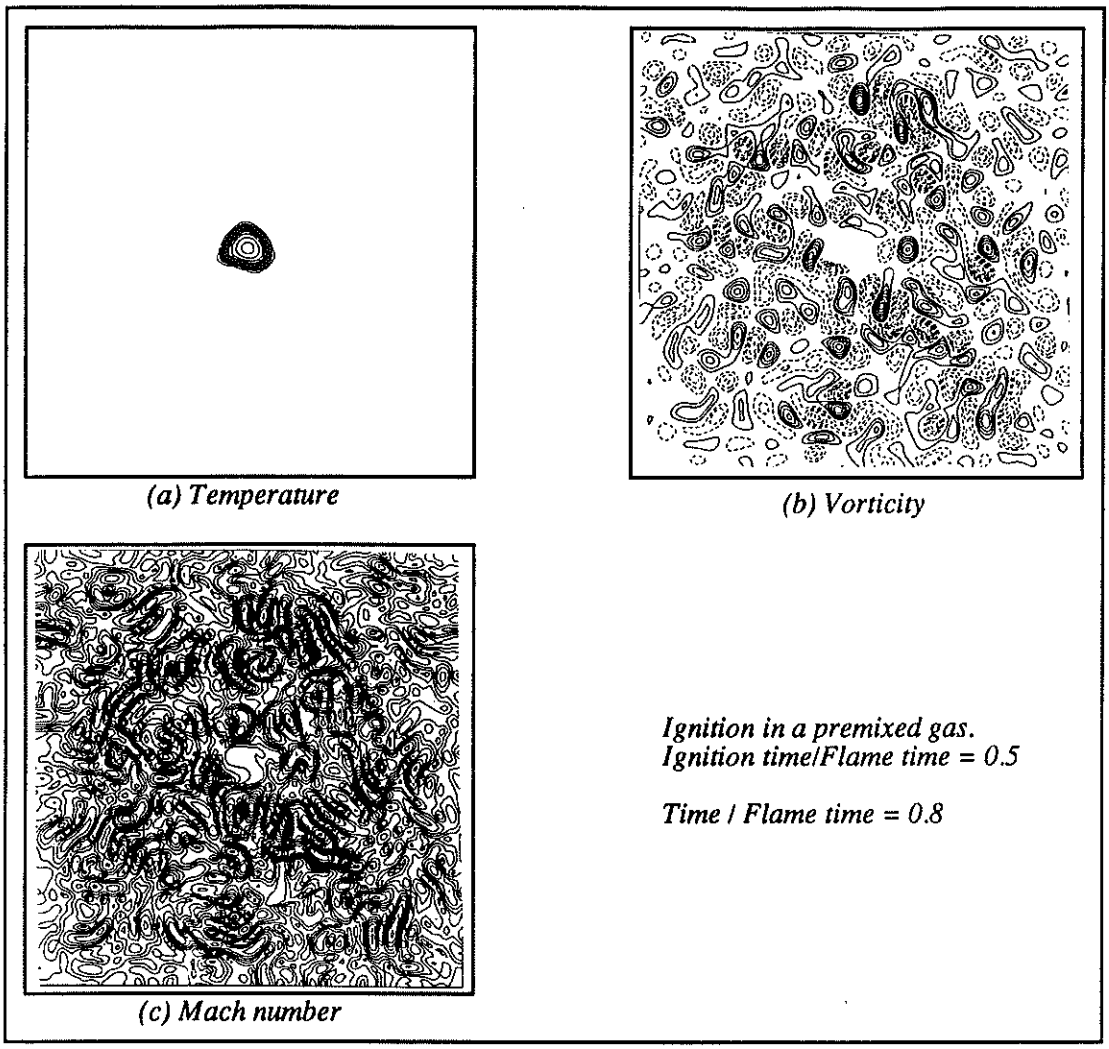

FIGURE 2. Ignition example for $Le = 1.2$: $t/t_{flame} = 0.8$

The spark creates a flame which grows first in a laminar-like fashion (Figure 1 and 2) and later transitions to a turbulent flame (Fig. 3 and 4). This result confirms experimental findings which describe the initial growth of the flame as an essentially laminar process (Baritaud (1989)). However, it is important to realize that this initial growth is controlled first by the large energy deposited by the spark which feeds the temperature field and helps it grow beyond the critical size needed for self-sustaining reaction to occur.

During the first instants, a weak shock wave is initiated by the ignition and may be seen on the Mach number fields in Figures 1 and 2. The velocity difference due to dilatation through the flame front is also visible on Fig. 1 but may not be seen at later times because turbulent fluctuations overcome it. This confirms that the initial growth of the flame is controlled by its own dilatation which is always larger than the turbulent fluctuations and isolates the flame core from the surrounding turbulence. Later, when the flame gets larger, it becomes more difficult for the laminar propagation to overcome turbulent fluctuations and transition to turbulent propagation occurs. This may be also characterized in terms of flame stretch as shown in Section 5.

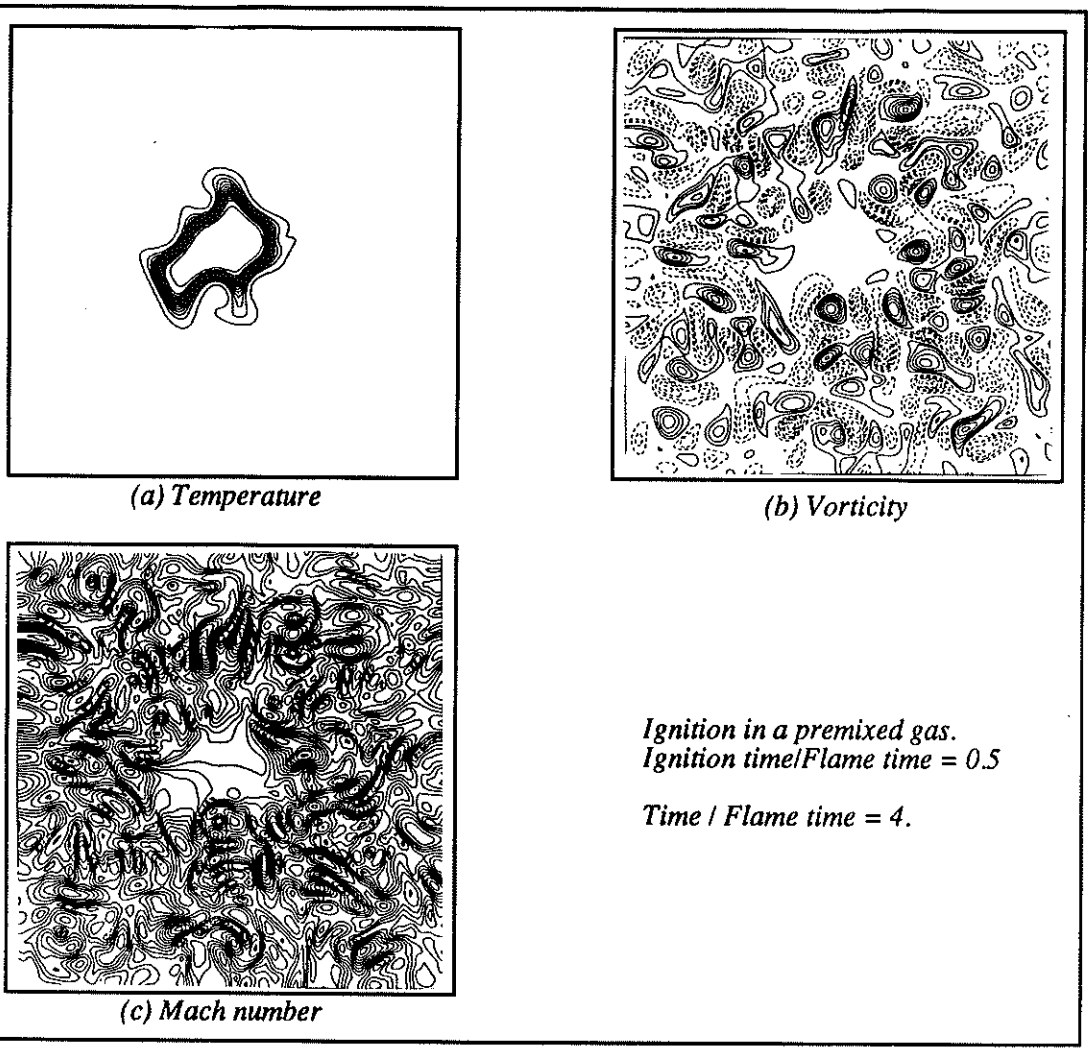

FIGURE 3. Ignition example for $Le = 1.2$: $t/t_{flame} = 4$.

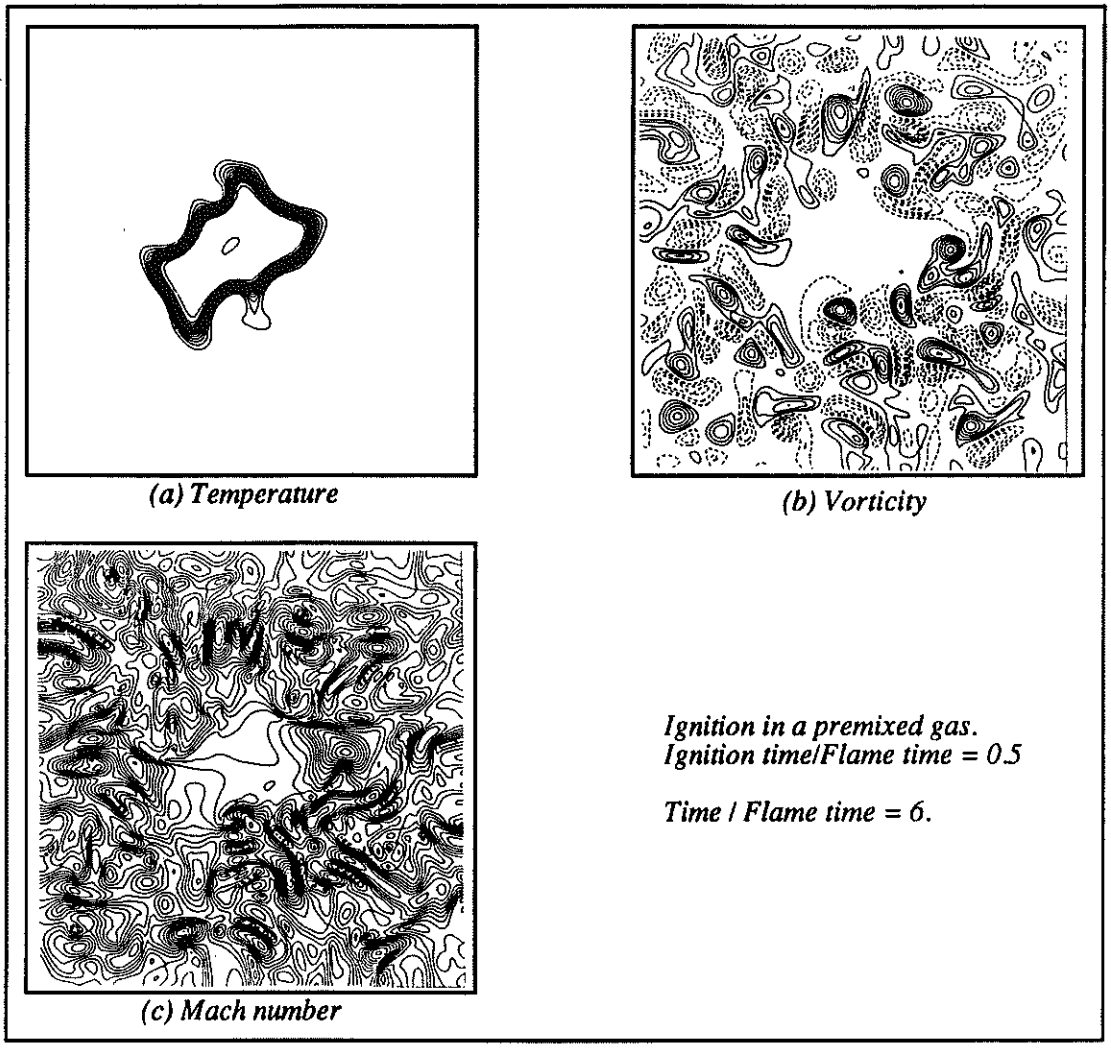

FIGURE 4. Ignition example for $Le = 1.2$: $t/t_{flame} = 6$.

The effect of the flame on turbulence is strong: vorticity is reduced to low levels inside the burnt gases. This is due both to dilatation (the density is four times smaller in the burnt core) and large viscosity (the kinematic viscosity is about 10 times larger in the burnt core than in the fresh gases).

4. Numerical tests

4.1. Effects of boundary conditions

Initial turbulent fluctuations are imposed using a specified spectrum (Lee et al. (1991)). These initial fluctuations are usually periodic over the two computation directions and constitute the initial velocity field.

One of the main problems of the present simulation is the impossibility of maintaining periodicity during the computation and therefore of using periodic boundary conditions. Because of dilatation, combustion creates an outward mean motion which pushes fresh gases out of the computation domain and prohibits any periodicity assumption. At first sight there is some advantage to this situation because most of the velocities will correspond to flow leaving the computation box (a case which is easier to treat, see Poinsot and Lele (1991)). However, in the turbulent case, speeds corresponding to flow entering the domain may also be generated and maintained for a long time even though combustion takes place in the box. In this case, we clearly lack information to update these velocities on all sides of the domain.

Different tests of the boundary conditions performances were performed in the case of decaying turbulence without combustion. This is a more difficult test because no dilatation is present to induce outgoing movement near the boundaries. If the standard non-reflecting NSCBC method is used for all boundaries and turbulent fluctuations are imposed everywhere in the domain, some non-physical results may be obtained: large ingoing velocities are maintained on boundaries for long times so that the RMS velocity decreases but then increases again. To overcome this difficulty, the initial turbulent fluctuations may be imposed only in the center of the box and clipped near the boundaries using a spatial filter. For this study the following filter was used:

$$f(x,y) = [cos(\pi(x - X_{max}/2)/X_{max}) * cos(\pi(y - Y_{max}/2)/Y_{max})]^{0.2} \qquad (10)$$

where the computation domain goes from 0 to X_{max} for x and from 0 to Y_{max} for y.

The efficiency of the NSCBC boundary conditions combined with the clipping of initial turbulence near the boundaries may be assessed by comparing decaying turbulence in a perfectly periodic domain (with periodic boundary conditions and no initial clipping) with decaying turbulence in a non periodic domain (with NSCBC conditions and initial clipping). This is done in Fig. 5 for an initial RMS velocity $u'/c = 0.1$ (c is the sound speed) and a reference length scale $L_i/L = 0.7$ (L is the unit length in the code given by the Reynolds number $Re = Lc/\nu$). The box size is 9 by 9 and the grid is 257 by257.

Figure 5 presents time variations of the kinetic turbulent energy k and dissipation ϵ. Full symbols correspond to the NSCBC case while hollow symbols designate the perfectly periodic case. An integral turbulent time τ is defined as

$$\tau = c_0 k/\epsilon = l_2/\sqrt{k}, \qquad (11)$$

where c_0 is a constant depending on the spectrum shape and was fixed to 0.4 here.

The solid line and the dashed line indicate the prediction of a simple model for k/k_0 and ϵ/ϵ_0 based on the classical equations for decaying turbulence (k_0 and ϵ_0 are the initial values of k and ϵ, τ_0 is the initial integral time $\tau_0 = c_0 k_0/\epsilon_0$):

$$\frac{\partial k}{\partial t} = -\epsilon \qquad \text{and} \qquad \frac{\partial \epsilon}{\partial t} = -C_2 \frac{\epsilon^2}{k}. \qquad (12)$$

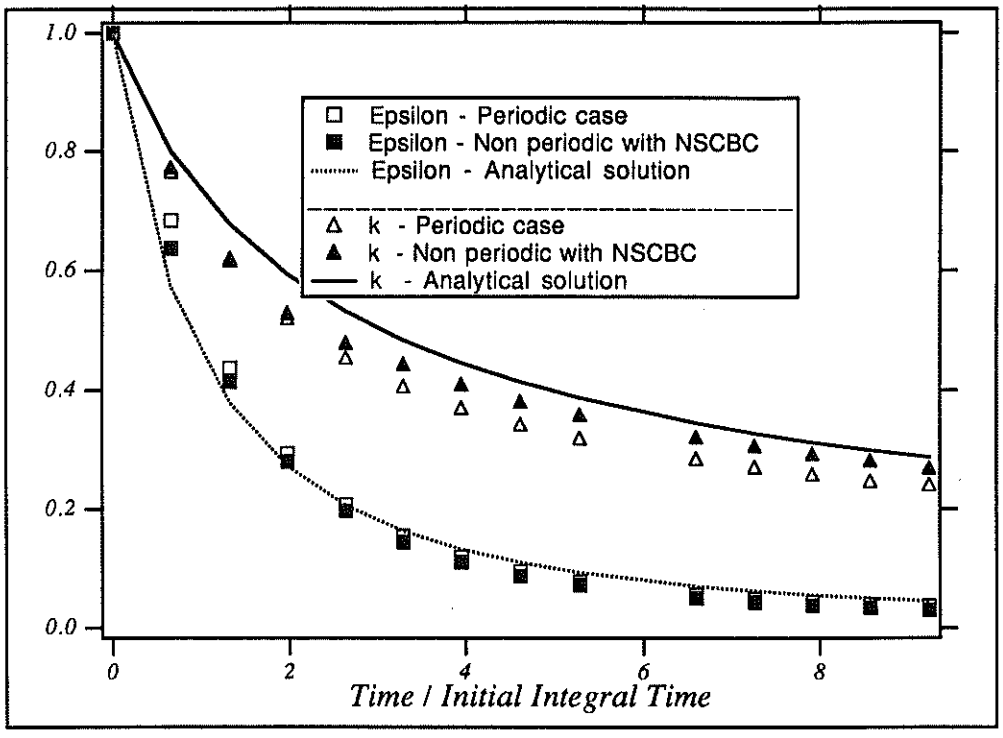

FIGURE 5. Variation of the turbulent kinetic energy k and of the dissipation ϵ for cold flow computations (Comparison between a periodic case, a NSCBC computation with clipping and the analytical solution).

These equations may be solved easily to obtain:

$$\frac{k}{k_0} = (1 + c_0(C_2 - 1)\frac{t}{\tau_0})^{-1/(C_2-1)}, \tag{13}$$

$$\frac{\epsilon}{\epsilon_0} = (1 + c_0(C_2 - 1)\frac{t}{\tau_0})^{-C_2/(C_2-1)}, \tag{14}$$

$$\frac{\tau}{\tau_0} = 1 + c_0(C_2 - 1)\frac{t}{\tau_0}. \tag{15}$$

The integral turbulent time τ is quite important for turbulent combustion modeling because it controls the characteristic time for flame stretching (Cant and Bray (1988), Meneveau and Poinsot (1991), Mantel and Borghi (1991)). Figure 6 shows the variations of τ with time for the periodic case (empty squares), the NSCBC case (full squares) and the theoretical function given by Eq. (15) (solid line).

Figures 5 and 6 show that the non periodic case computed with the NSCBC method and a clipping of turbulence near boundaries behave like the periodic case and that both cases behave like the theoretical solutions when a value of 2.5 is taken for the constant C_2. Although this value is higher than the commonly used value $C_2 = 1.92$, it is still quite reasonable for two-dimensional turbulence initialized with

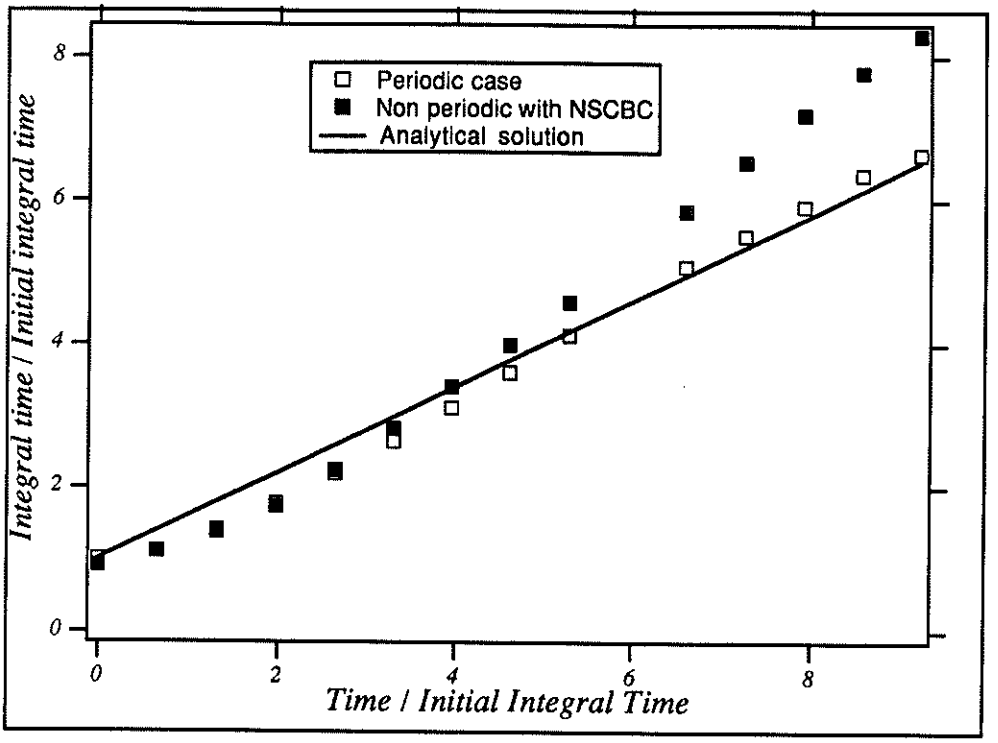

FIGURE 6. Variation of the turbulent integral time for cold flow computations (Comparison between a periodic case, a NSCBC computation with clipping and the analytical solution).

random conditions. Tests indicate that such an agreement may be obtained only when the integral length is not too large. For reference lengths L_i larger than 0.2 times the box size, turbulence evolves correctly for two or three turnover times but drifts later to a non realistic behavior. When L_i is smaller than 0.2 times the box size, the evolution of turbulence is satisfactory and the values of C_2 obtained for different runs vary between 2.4 and 3. The turbulent length scale $l_2 = c_0 k^{3/2}/\epsilon$ is plotted in Fig. 7.

The fact that turbulence behaved correctly immediately after the beginning of the runs lead us to start flame ignition right away and therefore to take $t_{delay} = 0$ in this first study (Because of the finite time required for ignition, the flame actually starts burning only after a time which is of the order of a turnover time in most cases).

4.2. Effects of initial turbulence conditions

To produce meaningful comparisons between DNS results, which correspond to one individual flow realization and model results, which predict values averaged over a large number of flow realizations, the question of repeatability of DNS results must be considered. It was addressed here by running the same ignition problem with different initial seeds. It was found that most runs behaved the same way, providing

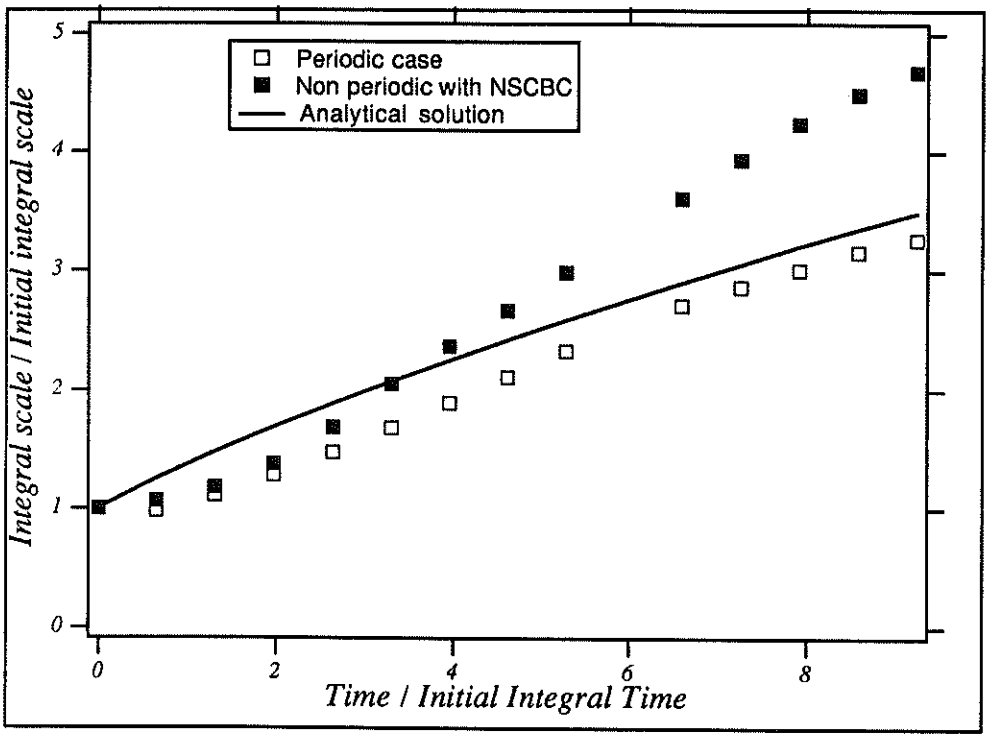

FIGURE 7. Variation of the turbulent length scale with time for cold flow computations (Comparison between a periodic case, a NSCBC computation with clipping and the analytical solution).

a scatter of only 10 percent in terms of mean reaction rate, except for cases where a 'catastrophic ' event would occur. Figure 8 shows the variations of the total reaction rate for runs V4,V8,V9 and V10 performed with $u'/c = 0.1$ and $L_i/L = 0.7$ (see Tables I and II).

The total reaction rate is plotted in terms of an 'equivalent flame radius' which is the radius of a circular laminar flame moving at speed s_L^0 and having the same reaction rate as the turbulent flame. This radius integrates effects of flame wrinkling as well as local flame speed variations.

Case V10 is characterized by the occurence of a catastrophic event for the flame growth after two turn-over times: this event corresponds to the separation of a burnt pocket from the main bulk and to the subsequent extinction of this pocket as shown in Fig. 9. After this event the growth of the flame resumes with a slope close to the other cases. Note that in other simulations pockets of burnt gases are formed but do not quench at later times: there is no apparent rule governing the quenching of these pockets (except for the evident limit of being larger than the critical ignition size).

Altogether, it appears that the four runs shown in Fig. 8 are quite close even though case V10 is propably not representative of the mean evolution. This suggests that only a few runs on a given case with different random initial conditions should

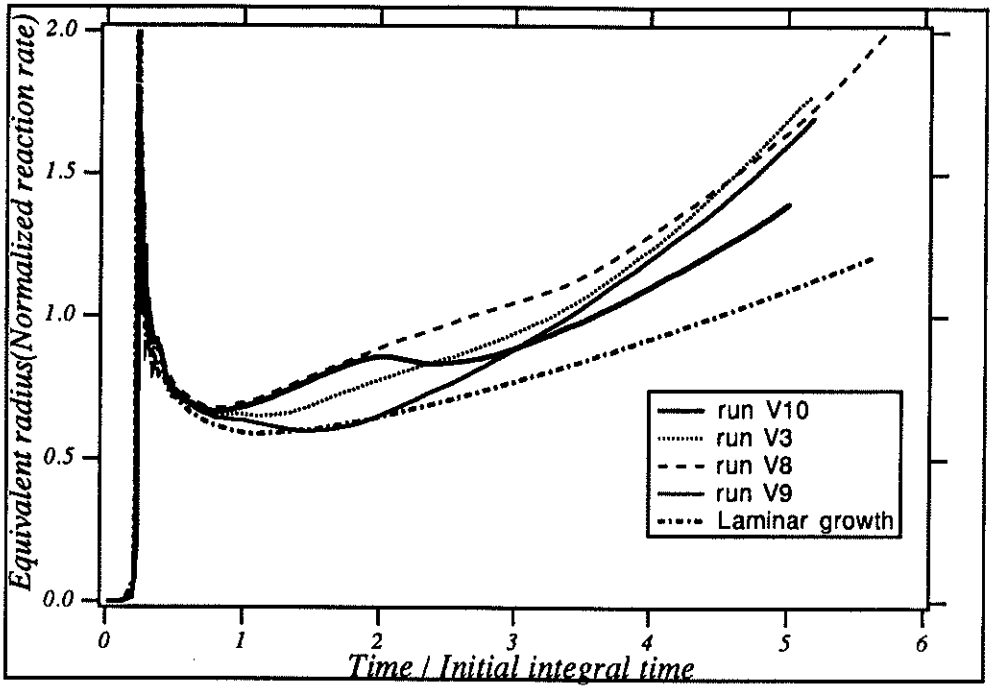

FIGURE 8. Comparison between four runs with different random initial conditions (Runs V4, V8,V9 and V10).

provide a meaningful average evolution.

5 Effects of Lewis number and molecular effects

5.1 Flame stretching during laminar kernel growth

Contrary to classical flame propagation, turbulent and laminar ignition processes are dominated (at least initially) by a stretch which is generated by the growth of the flame itself. Flame stretch can be expressed as (Candel and Poinsot (1990)):

$$S = \frac{1}{\Sigma}\frac{\partial \Sigma}{\partial t}, \tag{16}$$

where Σ is the flame surface.

In the case of a two-dimensional laminar flame ignited at a point source, the flame first starts and after the initial ignition process grows at a constant speed (Champion et al. (1986)). This speed is the flame displacement speed and is given by the growth of the flame radius $\frac{\partial r}{\partial t}$ (Poinsot et al. (1991))

$$\frac{\partial r}{\partial t} = \frac{T_2}{T_1} s_L, \tag{17}$$

where s_L is the consumption speed of the flame so that its surface $\Sigma = 2\pi r$ is characterized by a stretch:

$$S = \frac{1}{r}\frac{\partial r}{\partial t} = \frac{T_2}{T_1} s_L / r, \tag{18}$$

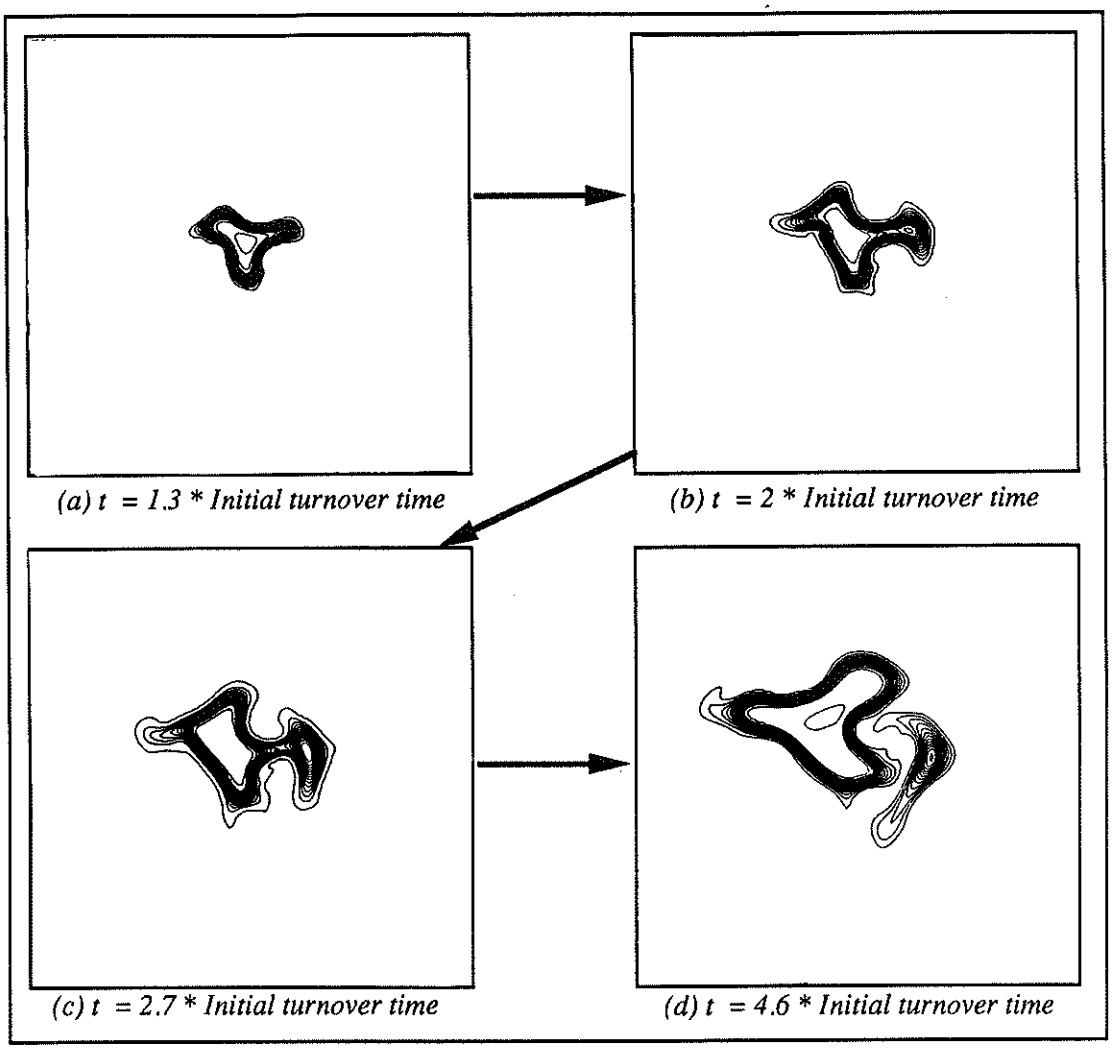

FIGURE 9. Example of 'catastrophic' event during flame growth: a pocket of burnt gases is produced and quenched.

This laminar stretch is large when the flame radius is small and one of its effects is to modify the consumption speed s_L (which is sensitive to stretch when the Lewis number is not unity). The flame speed s_L increases for positive stretch when $Lewis < 1$ and decreases when $Lewis > 1$. The effects of stretch during laminar flame growth are demonstrated in Fig. 10 and 11 for two flames with $Lewis = 1.2$ and $Lewis = 0.53$.

Figure 10a and 11a present variations of the total reaction rate (normalized as an equivalent radius) and of the flame radius r. Figure 10b and 11b show the variations of the consumption speed (normalized by s_L^0) and of the flame stretch normalized by the critical stretch s_L^0/δ_{l1}.

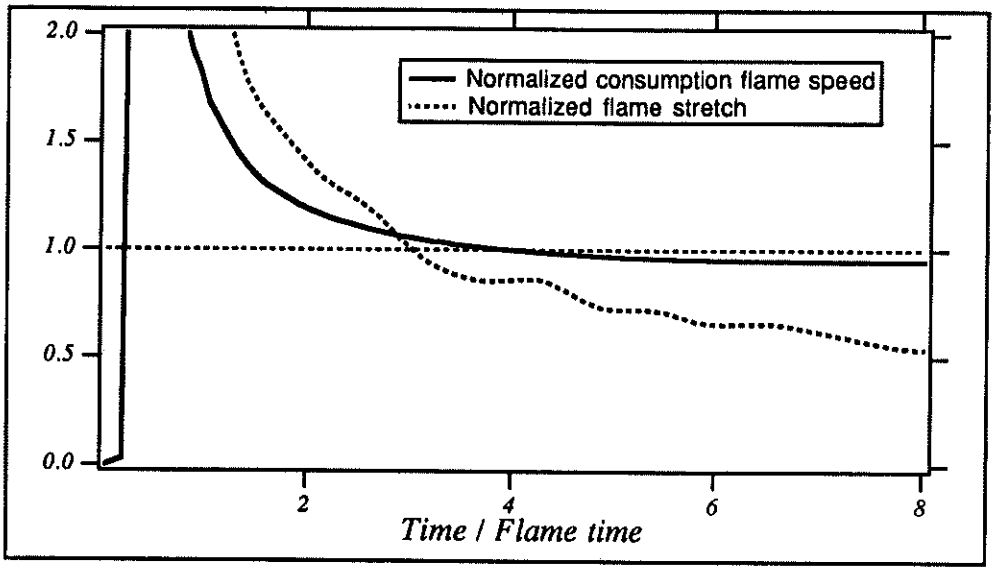

FIGURE 10A. Total reaction rate and flame radius r versus time for the *Lewis* = 1.2 flame (laminar case).

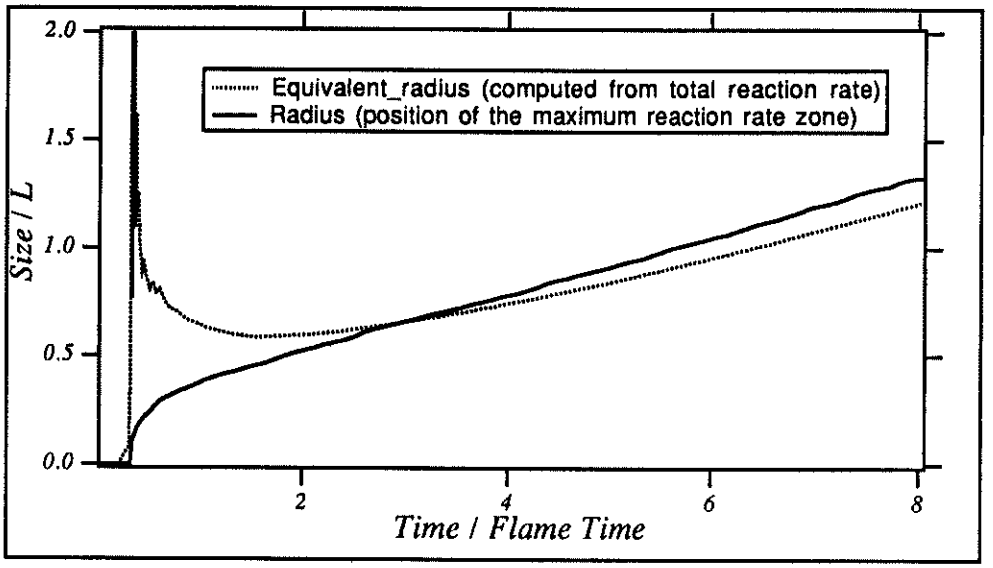

FIGURE 10B. Consumption speed s_L/s_L^0 and flame stretch $S/(s_L^0/\delta_{l1})$ for the *Lewis* = 1.2 flame (Laminar case)

The *Lewis* = 0.53 flame grows much faster (Fig. 11) than the *Lewis* = 1.2 flame (Fig. 10). The *Lewis* = 0.53 flame is characterized by a consumption flame speed which remains always larger than s_L^0 (Fig. 11b) because of stretch effects . In the case of the *Lewis* = 1.2 flame, the initial ignition phase leads to large values of the

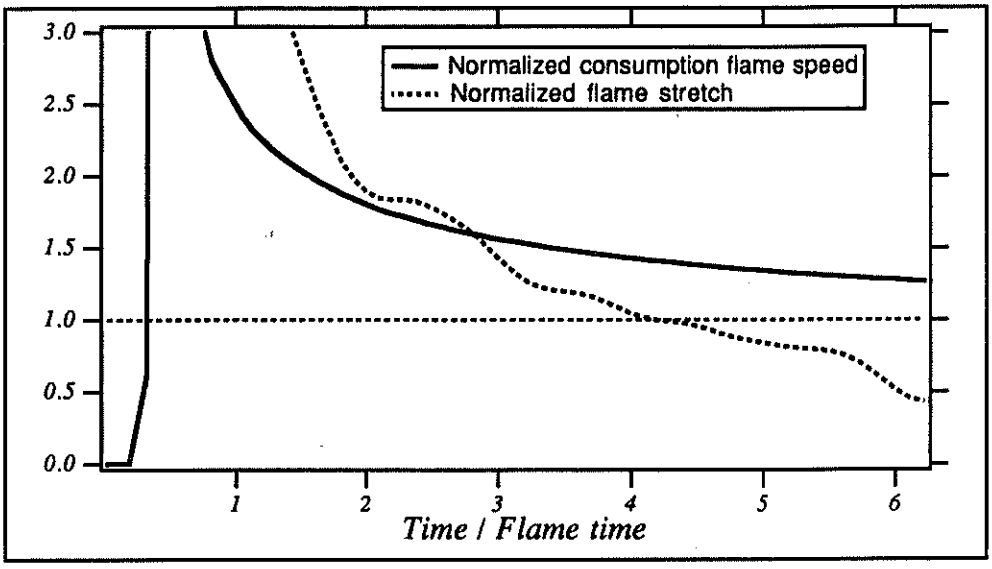

FIGURE 11A. Total reaction rate and flame radius r versus time for the *Lewis* = 0.53 flame (Laminar case).

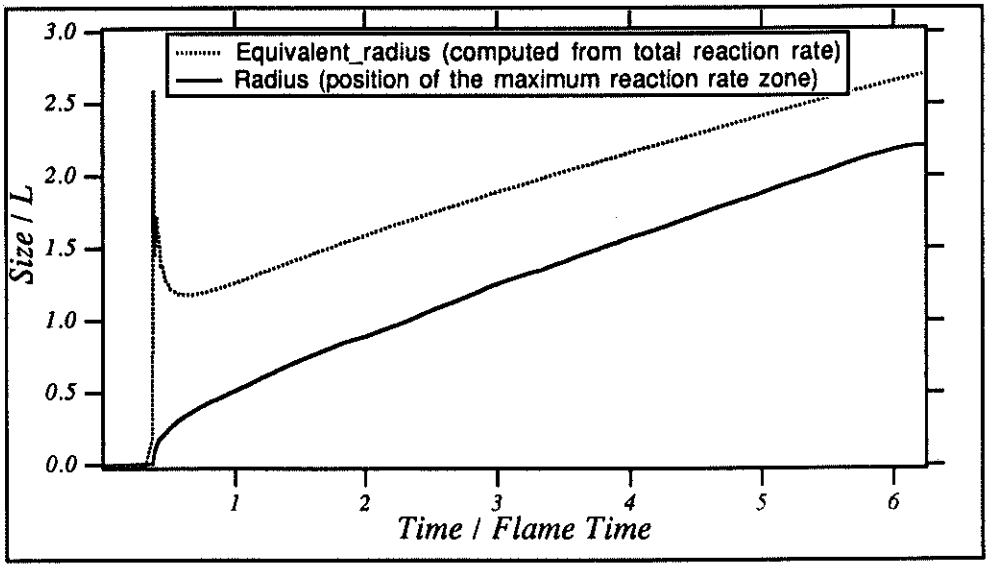

FIGURE 11B. Consumption speed s_L/s_L^0 and flame stretch $S/(s_L^0/\delta_{l1})$ for the *Lewis* = 0.53 flame (Laminar case).

consumption speed but as the flame relaxes to the structure of a stretched laminar flame, this quantity becomes less than the unstretched laminar flame speed s_L^0. For both flames, consumption speeds eventually relax to their unstretched values when the flame radius r is large enough and the reduced stretch decrease to values less

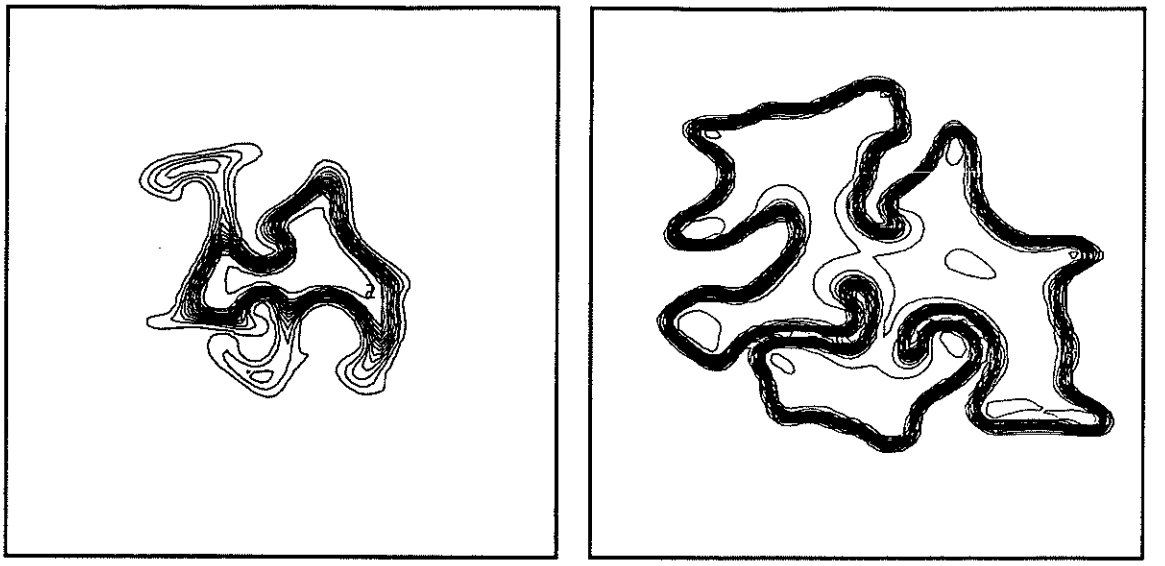

(a) Lewis = 1.2 - stable (b) Lewis = 0.53 - unstable

FIGURE 12. Temperature field at the same instant ($t = 4$ initial turn-over times) for run V8 (Lewis = 1.2) and run W4 (Lewis = 0.53)

than unity. Note the characteristic behavior of the *Lewis* = 0.53 flame: if it grows fast, it experiences a larger stretch and therefore a larger consumption speed leading to a faster growth and so on.

This simple result suggests that in turbulent cases, important quantities will be (1) the laminar stretch S defined above and created by the flame itself and (2) the turbulent stretch imposed on the flame by turbulent fluctuations.

Initially, the laminar stretch is always large and dominates the turbulent stretch. Later, if turbulence does not decay too fast (which is always the case in practical situations), the turbulent stretch overcomes the laminar stretch (which decreases like $1/r$) and leads to transition to turbulent propagation. However, the effects of turbulence are multiplied by another mechanism: the wrinklings created by vortices on the flame front trigger natural instabilities for *Lewis* = 0.53 and enhance the flame growth by creating large flame folding as shown in the next section.

5.2 Thermodiffusive instabilities during turbulent flame growth

The existence of flame instabilities for small Lewis numbers has been known for a long time (Williams (1988)). For Lewis numbers less than unity, differential diffusion between heat and species leads to the formation of cells on flame fronts: lower burning rate are found for elements concave towards reactants; higher burning rates for elements concave towards products. Therefore, flame deformations tend to increase and such flames become highly convoluted.

Although the influence of Lewis number is typically a molecular effect, it has been

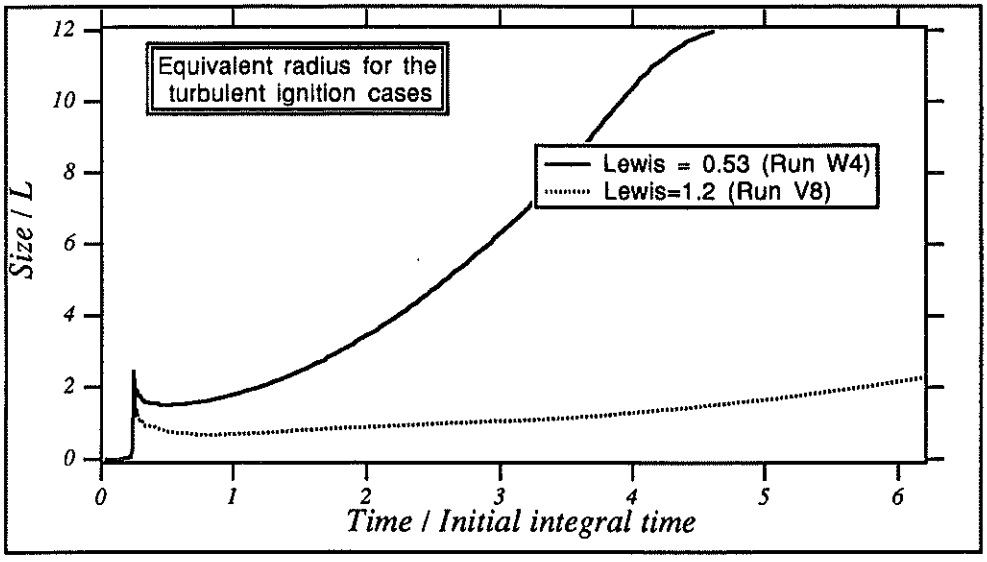

FIGURE 13. Evolution of the equivalent radius (normalized total reaction rate) for run V8 (Lewis = 1.2) and run W4 (Lewis = 0.53). Turbulent ignition.

evidenced in many high-Reynolds number turbulent flames including experiments (Wu et al. (1991)) or two-dimensional direct simulations (Haworth and Poinsot (1991)). DNS performed in three or two-dimensional low Reynolds number cases (Ashurst et al. (1987), Rutland and Trouve (1990)) have also produced the same results. Flame ignition is especially sensitive to cellular instabilities because the flame kernel is continuously submitted to stretch (even in a laminar case, see Eq. (18)). In laminar flows, this leads to the natural formation of spectacular flame structures as shown by Sivashinsky (1977). It was therefore interesting to check whether our simulations would indicate any influence of this essentially molecular mechanism for a turbulent case.

The comparison between runs V8 (Lewis =1.2) and W4 (Lewis=0.53) is given in Fig. 12. The initial turbulent fields are the same (see Table I and II).

The turbulent flame with Lewis=0.53 grows much faster than the flame with Lewis =1.2. The variation of the total reaction rate vs time for the two cases is given in Fig. 13. The turbulent flame speed (which is the slope of the total reaction rate curve vs time) for run W4 is about 4 times larger than for run V4. Clearly, molecular effects have a very important role to play during ignition and models should account for this effect even at large Reynolds numbers.

6. Summary and conclusions

A Direct Numerical Simulation of flame ignition in a turbulent premixed gas has been described. The formulation is two-dimensional, includes heat release, compressibility, finite rate chemistry and high activation energy Arrhenius law for chemistry. Flame is initiated by locally depositing energy in a flow submitted to

decaying turbulence. The influence of numerical parameters such as boundary conditions or initialization of turbulence was determined. Results suggest that DNS can be used to obtain information on shock wave formation at ignition, flame structure, transition from laminar to turbulent flame propagation, effects of stretch and of molecular effects. It was shown that thermo-diffusive instabilities characterizing laminar flames with Lewis numbers less than unity also appear on turbulent flames and significantly enhance flame growth.

REFERENCES

ASHURST, W. T., PETERS, N., & SMOOKE, M. D. 1987 Numerical simulation of turbulent flame structure with non-unity Lewis number. *Combust. Sci. Tech.* **53**, 339-375.

BARITAUD, T. A. 1987 High speed schlieren visualization of flame initiation in a lean operating S.I. engine. *Int. Fuels and Lubricants Meet. and Exposition*, S. 872152.

BARITAUD, T. A. 1989 Combustion and fluid dynamic measurements in a spark ignition engine: effects of thermochemistry and velocity field; turbulent flame speeds. *Int. Fuels and Lubricants Meet. and Exposition*, SAE Paper 892098.

BOSTON, P. M., BRADLEY, D., LUNG, F. K. K., WINCE, I. M., & WEINBERG, F. J. 1984 Flame initiation in lean, quiescent and turbulent mixtures with various igniters. *20th Symposium (Int.) on Combustion*, The Combustion Institute, Pittsburgh, 141-149.

CANDEL, S. & POINSOT, T. 1990 Flame stretch and the balance equation for the flame area. *Combust. Sci. Tech.* **70**, 1-15.

CANT, R. S. & BRAY, K. N. C. 1988 Strained laminar flamelet calculations of premixed turbulent combustion in a closed vessel. *22nd International Symposium on Combustion*, The Combustion Institute, Pittsburgh, 791.

CHAMPION, M., DESHAIES, B., JOULIN, G., & KINOSHITA, K. 1986 Spherical flame initiation : theory versus experiments for lean propane-air mixtures. 65, 319-337.

CHAMPION, M., DESHAIES, B., & JOULIN, G. 1988 Relative influences of convective and diffusive transports during spherical flame initiation. 74, 161-170.

FRENDI, A. & SIBULKIN, M. 1990 Dependence of minimum energy on ignition parameters. 73, 395-413.

HAMAI, K., KAWAJIRI, H., ISHIZUKA, T. & NAKAI, M. 1986 Combustion fluctuation mechanism involving cycle-to-cycle spark ignition variation due to gas flow motion in S.I. engines. *21st Symposium (Int.) on Combustion*, The Combustion Institute, Pittsburgh, 5O5-512.

HAWORTH, D. C. & POINSOT, T. J. 1990 The influence of Lewis number and nonhomogeneous mixture on premixed turbulent flame structure. *Proceedings of*

the Summer Program, NASA Ames-Stanford University Center for Turbulence Research, 281-298.

HAWORTH, D. C. & POINSOT, T. J. 1992 Numerical simulations of Lewis number effects in turbulent premixed flames. *J. Fluid Mech.* submitted for publication.

HERRING, J. R., ORSZAG, S. A. & KRAICHNAN, R. H. 1974 Decay of two–dimensional homogeneous turbulence. *J. Fluid Mech.* **66**, 417-444.

KO, Y. & ARPACI, V. S. 1991 Spark ignition of propane-air mixtures near the minimum ignition energy : Part II. A model development. 1991, 88-105.

KO, Y., ANDERSON, R. W. & ARPACI, V. S. 1991 Spark ignition of propane-air mixtures near the minimum ignition energy. Part I. An experimental study. 83, 75-87.

LEE, S., LELE, S. & MOIN, P. 1991 Eddy shocklets in decaying compressible turbulence. *Phys. Fluids A.* **3**(4), 657-664.

LELE, S. K. 1989 Direct numerical simulation of compressible free shear flows. *27th Aerospace Sciences Meeting,* AIAA 89-0374.

LESIEUR, M., *Turbulence in Fluids.* Martinus Nijhoff, 1987.

MALY, R. & VOGEL, M. 1978 Initiation and propagation of flame fronts in lean CH4-air mixtures by the threemodes of the ignition spark. *17th Symposium (Int.) on Combustion,* The Combustion Institute, Pittsburgh, 821-831.

MALY, R. 1981 Ignition model for spark discharges and the early phase of flame front growth. *18th Symposium (Int.) on Combustion,* The Combustion Institute, Pittsburgh, 1747-1754.

MANTEL, T. & BORGHI, R. 1991 A new model of premixed wrinkled flame propagation based on a scalar dissipation equation. *13th ICDERS Meeting.*

MENEVEAU, C. & POINSOT, T. 1991 Stretching and quenching of flamelets in premixed turbulent combustion. *Combust. Flame,* in press.

PISCHINGER, S. & HEYWOOD, J. B. 1990 A model for flame kernel development in a spark-ignition engine. *23rd Symposium (Int.) on Combustion,* The Combustion Institute, Pittsburgh, 1033-1040.

POINSOT, T., VEYNANTE, D. & CANDEL, S. 1991 Quenching processes and premixed turbulent combustion diagrams. *J. Fluid Mech.* **228**, 561-605.

POINSOT, T. & LELE, S. 1991 Boundary conditions for direct simulations of compressible viscous flows. *J. Comput. Phys* in press.

POINSOT, T., ECHEKKI, T. & MUNGAL, M. G. 1991 A study of the laminar flame tip and implications for premixed turbulent combustion. *Combust. Sci. Tech,* in press.

POPE, S. B. & CHENG, W. K. 1986 Statistical calculations of spherical turbulent flames. *21st Symposium (Int.l) on Combustion,* The Combustion Institute, Pittsburgh, 1487.

RUTLAND, C. J. & TROUVE, A. 1990 Pre-mixed flame simulations for non-unity Lewis number. *Proceedings of the Summer Program,* NASA Ames-Stanford University Center for Turbulence Research, 299-309.

SIVASHINSKY, G. I. 1977 Diffusional-thermal theory of cellular flames. *Combust. Sci. Tech.* **15,** 137-146.

SLOANE, T. M. 1990 Numerical simulation of electric spark ignition in atmospheric pressure methane-air mixtures. 73, 367-381.

SLOANE, T. M. 1990 Energy requirements for spherical ignitions in methane-air mixtures at different equivalence ratios. 73, 351-365.

THOMAS, A. 1986 The development of wrinkled turbulent premixed flames. *Combust. Flame.* **65,** 291-312.

TROMANS, P. S. & FURZELAND, R. M. 1986 An analysis of Lewis number and flow effects on the ignition of premixed gases. *21st Symposium (Int.) on Combustion,* The Combustion Institute, Pittsburgh, 1891-1897.

WILLIAMS, F. A., *Combustion Theory.* Benjamin Cummings, Menlo Park, CA, 1985.

WU, M. S., KWON, S., DRISCOLL, J. F., & FAETH, G. M. 1991 Preferential diffusion effects on the surface structure of turbulent premixed hydrogen/air flames. 78, 69-96.